JOURNAL OF AIRCRAFT
Vol. 30, No. 4, July–Aug. 1993

Time Domain Panel Method for Wings

Max Blair*
Wright Research and Development Center, Wright-Patterson Air Force Base, Ohio 45433
and
Marc H. Williams†
Purdue University, West Lafayette, Indiana 47907

A computer algorithm and Fortran code have been developed to simulate a time history of aerodynamic loads on planar lifting surfaces using the subsonic linearized potential integral formulation of Guderley.[1,2] This work is intended for application to the simulation of flexible wing motion with active controls. In this article the method is validated by examining the indicial responses of wings. The results are transformed to the frequency domain and compared to the results of a frequency domain doublet-lattice code H7WC.[3]

Introduction

THERE is a requirement for unsteady aerodynamics in vehicle dynamics analyses when the period of wing oscillation is less than or comparable to the time required to establish steady-state pressures. The subsonic and supersonic flutter problems have been successfully addressed with linear potential aerodynamics. For linear flutter analysis, a simple harmonic assumption is adequate and economical (since only a few frequencies are normally required). Frequency domain aerodynamic forces have also been used as a basis for time domain aerodynamic simulations.[3] Given a generalized aerodynamic force over a sufficiently wide frequency range, it is possible to approximate the time dependent loads which arise with arbitrary motion by using an inverse Fourier transform. In practice, the harmonic aerodynamic loads for a given mode are generated for a finite set of frequencies. This discrete harmonic data is then curve-fit (e.g., with rational functions of frequency) and analytically transformed into the time domain. Such procedures are very indirect and subject to considerable modeling uncertainties.

The subject of this article is the development of direct time domain aerodynamics based on the integral formulation of Guderley.[1,2] A thin wing is modeled with a single-source doublet sheet. This exact velocity potential formulation is especially appealing because there is no singularity in the integrand. While Ref. 1 presents the original derivation, some simplification to the derivation is provided in Ref. 2. The resulting formula is the same in both references.

Time domain unsteady aerodynamics are useful in control and gust response problems. This is especially true for vehicles with nonlinear dynamics or nonlinear controls. Examples of nonlinear controls are the active adaptive control of flutter and nonsynchronous digital controls. Examples of nonlinear dynamics include rigid body motion, nonlinear actuators, buckled structure, freeplay, and friction. All of these nonlinear examples may be simulated with linear aerodynamics. Furthermore, as an alternative to methods such as Ref. 4, it may be economical to obtain Laplace or harmonic aerodynamic forces from indicial functions which were obtained with linear time domain aerodynamics.

Presented as Paper 89-1323 at the AIAA/ASME/ASCE/AHS/ASC 30th Structures, Structural Dynamics and Materials Conference, Mobile, AL, April 3–5, 1989; received May 15, 1989; revision received April 6, 1992; accepted for publication May 5, 1992.

*Aerospace Engineer. Senior Member AIAA.
†Professor of Aerospace Engineering, School of Aeronautics and Astronautics. Member AIAA.

Guderley[1] proposed solving the linearized wave equation (in terms of the velocity potential) directly in the time domain for nonlinear aeroservoelastic simulation in 1985. The result is the integral Eqs. (5) and (6) of this report. The time domain panel (TDP) method is a discretized implementation of Eqs. (5) and (6). Guderley's integral formulas are exact expressions for the normal flow induced by a planar doublet sheet. The TDP method is a subsequent development which adds numerical errors that are due to discretizations. The accuracy of the TDP method is investigated in this report by comparing the results with those from Ref. 3 and using a systematic variation in the number of elements. Subsequent aeroelastic applications of the TDP method were presented by Blair et al.[5,6]

The time domain aerodynamic loads on wings were first studied in Ref. 7 by investigating the indicial response on an impulsively loaded wing. The circulatory and noncirculatory contributions to the indicial response are readily identified. Only thin two-dimensional airfoils were addressed for subsonic flows.

In Ref. 8, a panel method based on Green's theorem was used to model unsteady subsonic compressible aerodynamics in terms of the velocity potential for general configurations. This capability to model loads due to arbitrary motion was incorporated in the program, SOUSSA ACTS. Wing thickness was modeled with panels on the top and bottom surface. In unsteady lifting surface theory, one assumes the effect of wing thickness is a steady problem which can be calculated independently. In accounting for the top and bottom surfaces separately, the number of unknowns (e.g., the unknown doublet strength at points on the surface) is double the number for a single surface. Therefore, the fact that Ref. 8 must model wing thickness may be an undesirable feature. On the other hand, infinitely thin wings in subsonic flow are addressed by the TDP method with a single surface. This represents a significant computational advantage.

The algorithms described in Refs. 9 and 10 use a time domain integral formulation in direct pressure form for general configurations in an atmospheric fixed coordinate system. In Ref. 10, the singular integral is numerically evaluated over subareas with quadratures. For the subarea in which the integrand is singular, the algorithm assumes the pressure is constant and uses a Cauchy principle value interpretation to evaluate the integral analytically. The results include the effect of wing thickness, which for this linear analysis adds unnecessary numerical complication as far as the time-dependent component of pressure is concerned. The algorithm described in Ref. 9 utilizes a lattice approach, but only supersonic results are presented.

As a final note, the TDP method may be different from other panel methods in the sense that all panels are not treated

identically. Here, panels are treated according to their proximity to the control point and the wing boundary. Control points are located at the corners of the panels. Those panels which surround the control point use a nonsingular integral formulation over the surrounding panels as a group. The panels which are not adjacent to the control point use a different and singular integral formula. This is discussed in the following section.

TDP Method

As indicated, Guderley's formula is an integral solution to the classical small disturbance potential boundary value problem (bvp) for compressible flow. Here, the orthogonal axes are in uniform translation with respect to the atmosphere with velocity $-U_i$ The axes are measured with (x, y, z) coordinates:

$$\beta^2\phi_{xx} + \phi_{yy} + \phi_{zz} - (2M/a)\phi_{xt} - (1/a^2)\phi_{tt} = 0 \quad (1)$$

The velocity potential is ϕ, a is the freestream speed of sound, M is the freestream Mach number, and $\beta = \sqrt{1 - M^2}$. The tangential flow boundary condition and the Kutta condition are imposed. An excellent discussion of the fundamental solutions to Eq. (1) is presented by Garrick.[11] Given a thin wing in the $z = 0$ plane, the present approach is to use a single sheet of source doublets to solve this bvp. The umbral variables (ξ, η) of integration are measured along the (x, y) axes. Whereas (x, y) are used to locate the control points, (ξ, η) are used within the integral to specify a location on the doublet sheet. Some important aspects of the integral formula are presented in the following paragraph. The remaining details of the derivation are given in Refs. 1 and 2.

Let

$$\begin{aligned} \boldsymbol{r} &= (\xi - x)\hat{i} + (\eta - y)\hat{j} \\ \rho_c &= \sqrt{(\xi - x)^2 + \beta^2(\eta - y)^2} \\ R_0 &= [\rho_c + M(\xi - x)]/\beta^2 \\ \boldsymbol{R} &= \boldsymbol{r} + MR_0\hat{i} \\ (t - \tau) &= (R_0/a) \end{aligned} \quad (2)$$

where $(t - \tau)$ is the time required for a wave to propagate from (ξ, η) to (x, y) in the $z = 0$ plane. Let $h(x, y, t)$ be the history of the doublet strength in the $z = 0$ plane. Define

$$\frac{Dh}{Dt} = U\frac{\partial h}{\partial x} + \frac{\partial h}{\partial t} \quad (3)$$

$$\boldsymbol{\gamma} = \boldsymbol{\gamma}(\xi, \eta, \tau_f) = h_\xi(\xi, \eta, \tau_f)\hat{i} + h_\eta(\xi, \eta, \tau_f)\hat{j} \quad (4)$$

where $\boldsymbol{\gamma}$ is vorticity. Here $h_\xi(\xi, \eta, \tau_f)$ is the derivative of h with respect to the first argument. The subscript f in τ_f indicates that τ is not considered a function of ξ for differentiation. One interprets $h_\eta(\xi, \eta, \tau_f)$ similarly. (The significance of holding τ constant with respect to the variable of differentiation is seen when one evaluates the $\boldsymbol{\gamma}$ term in the integral formula. Holding τ, as defined in Eq. (2), constant is not only exact, but it is also an added blessing encountered in the numerical evaluation.) For a thin wing in level flight (in the neighborhood of the $z = 0$ plane) at $M < 1$, the integral equation which relates the upwash $w(x, y, t)$ and the doublet history $h(x, y, t)$ is given by

$$w(x, y, t) = I_2 - \left(\frac{2\pi}{a}\right)\frac{Dh}{Dt} \quad (5a)$$

where

$$I_2 = \int\int_{A_f} (\boldsymbol{R}/R_0^2\rho_c)\cdot\boldsymbol{\gamma}\, d\xi\, d\eta \quad (5b)$$

and A_f includes both the planform and the planar wake area. Equation (5a) is singular at $\rho_c = 0$. This singularity can be removed. [One of the rules in the derivation of any integral formula for a lifting surface is to take the limit as z goes to zero at the appropriate time. In essence, this is how one removes the singularity from Eq. (5b).] For a region A_n, which is inclusive of the point $\rho_c = 0$, the nonsingular exact equivalent to Eq. (5b) is

$$I_2 = I_3 + I_4 \quad (6a)$$

where

$$I_3 = -\boldsymbol{\gamma}_c\cdot\oint_S \left(\frac{\hat{n}}{R_0}\right) dS \quad (6b)$$

$$I_4 = \int\int_{A_n} \left(\frac{\boldsymbol{R}\cdot(\boldsymbol{\gamma} - \boldsymbol{\gamma}_c)}{R_0^2\rho_c}\right) dA \quad (6c)$$

Here, $\hat{n}$ is the in-plane outward unit normal to the boundary of the region of integration. I_3 is evaluated along the boundary S of the region of integration A_n. The positive direction obeys the right-side rule about the $+z$ axis. The current value of $\boldsymbol{\gamma}$ at $\tau = t$, $\xi = x$ and $\eta = y$ is denoted by $\boldsymbol{\gamma}_c$

$$\boldsymbol{\gamma}_c = \boldsymbol{\gamma}(x, y, t) \quad (7)$$

A_f of Eq. (5a) is discretized with quadrilateral subareas. The vertices of the subareas not on the wing leading edge or wingtip serve as the control points where the upwash w is known on the wing. The control points coincide with the points of support of the doublet strength function h. Equation (5a) is numerically evaluated over quadrilateral subareas not adjacent to the control point. The doublet strength in these subareas are interpolated with a bilinear function. Numerical integration is performed with Gaussian quadratures. Equations (6a) and (6b) are evaluated over an area comprised of the four quadrilateral subareas which surround the control point. The doublet strength is interpolated over the central portion of this near area with one quadratic function. One can see, the integrand of I_4 is nonsingular in terms of polar coordinates. As ρ_c approaches zero, both the numerator and the denominator approach zero to the third power such that the integrand is a continuous function. Square root singularities in h are employed along wing boundaries except at the trailing edge. Zero pressure difference (Kutta condition) is enforced at the trailing edge and in the wake. The wake is truncated far downstream of the trailing edge for reasons of practicality. For the same truncation error, high aspect-ratio wings require more wake than low aspect-ratio wings. Thus, high aspect-ratio wings require more computer memory than low aspect-ratio wings. With the above discretization scheme, the doublet history $\{\boldsymbol{h}\}$ is related to the current upwash $\{\boldsymbol{w}\}$ by

$$\{\boldsymbol{w}\} = [A]\{\boldsymbol{h}\} = [A_0|A_1|A_2]\begin{pmatrix}\{\boldsymbol{h}_0\}\\ \{\boldsymbol{h}_1\}\\ \{\boldsymbol{h}_2\}\end{pmatrix} \quad (8)$$

$\{\boldsymbol{h}_0\}$ is the vector of the doublet strength at control points at the current time. $\{\boldsymbol{h}_1\}$ is the vector of the doublet strength at control points at the previous time step. The vector $\{\boldsymbol{h}_2\}$ contains the remaining doublet history. ($\{\boldsymbol{h}_1\}$ and $\{\boldsymbol{h}_2\}$ are partitioned for postprocessing convenience.) Equation (8) can be solved for $\{\boldsymbol{h}_0\}$ because all other quantities are known:

$$\{\boldsymbol{h}_0\} = [A_0]^{-1}(\{\boldsymbol{w}\} - [A_1]\{\boldsymbol{h}_1\} - [A_2]\{\boldsymbol{h}_2\}) \quad (9)$$

Consistent with the small deformation assumption, the $[A]$ matrix is independent of time and only needs to be evaluated once. The upwash $\{\boldsymbol{w}\}$ and the doublet vectors $\{\boldsymbol{h}_1\}$ and $\{\boldsymbol{h}_2\}$

are known at each time step. Therefore, the doublet strength $\{h_0\}$, can be directly computed with Eq. (9) with simple matrix multiplication and addition. After $\{h_0\}$ has been computed, this new information is used to update the doublet strength for the next time step.

The chosen time step is based on the time for a pressure wave to traverse one nominal size panel. (The Lorentz transform is suggested in Ref. 7. This has the effect of distorting the time scale such that upstream and downstream waves travel at the same speed. This brings some sense of symmetry into the simulation, but complicates the interpretation of the upwash and doublet strength in nondistorted time. The Lorentz transform is useful when the upwash is known a priori, but is not useful for direct incorporation into the simulation of vehicle dynamics.)

Once the doublet strength is known, the pressure jump across the wing can be computed by

$$p = -4\pi\rho\left(\frac{Dh}{Dt}\right) \tag{10}$$

Using numerical integration, one can compute the generalized forces $\{F\}$ for the simulation of vehicle dynamics in the time domain. If $\{h\}$ is interpolated piecewise linearly in time then $\{F\}$ takes the form

$$\{F\} = [C_0]\{h_0\} + [C_1]\{h_1\} \tag{11}$$

where $[C_0]$ and $[C_1]$ are constant matrices.

The remainder of this report is dedicated to aerodynamic correlation with Ref. 3. For this reason, the results are specialized to indicial and harmonic responses.

Indicial Aerodynamics

The TDP method assumes the wing remains in the neighborhood of the $z = 0$ plane. For this study, wing deformation away from the $z = 0$ plane, $g(x, y, t)$, is represented with a nondimensional function $\bar{g}(\bar{x}, \bar{y}, \bar{t}) = (1/b)g(x, y, t)$

$$\bar{g}(\bar{x}, \bar{y}, \bar{t}) = \sum_{j=1}^{4} a_j(\bar{t})\bar{x}^{m_j}\bar{y}^{n_j} \tag{12}$$

where $\bar{t}$ is (Ut/b), $\bar{x}$ is (x/b), $\bar{y}$ is (y/b), and b is some reference length to be specified. The sequences are defined by $m_j = \{0, 1, 2, 0\}$ and $n_j = \{0, 0, 0, 2\}$. The upwash function used in Eq. (5) is related to $g(\bar{x}, \bar{y}, \bar{t})$ by

$$\begin{aligned} w(\bar{x}, \bar{y}, \bar{t}) &= U\left(\frac{\partial \bar{g}}{\partial \bar{t}} + \frac{\partial \bar{g}}{\partial \bar{x}}\right) \\ &= U\bar{w}(\bar{x}, \bar{y}, \bar{t}) \end{aligned} \tag{13}$$

The function $\bar{w}(\bar{x}, \bar{y}, \bar{t})$ is nondimensional. In terms of Eq. (12)

$$\begin{aligned} \bar{w}(\bar{x}, \bar{y}, \bar{t}) &= \dot{a}_1(\bar{t}) + \dot{a}_2(\bar{t})\bar{x} + \dot{a}_3(\bar{t})\bar{x}^2 \\ &\quad + \dot{a}_4(\bar{t})\bar{y}^2 + a_2(\bar{t}) + 2a_3(\bar{t})\bar{x} \end{aligned} \tag{14}$$

For the problem at hand, it will be sufficient to model the upwash function with the superposition of four functions:

$$\begin{aligned} \bar{w}(\bar{x}, \bar{y}, \bar{t}) &= u_1(\bar{t}) + u_2(\bar{t})\bar{x} + u_3(\bar{t})\bar{x}^2 + u_4(\bar{t})\bar{y}^2 \\ &= u_1(\bar{t})\bar{w}_1(\bar{x}, \bar{y}) + u_2(\bar{t})\bar{w}_2(\bar{x}, \bar{y}) \\ &\quad + u_3(\bar{t})\bar{w}_3(\bar{x}, \bar{y}) + u_4(\bar{t})\bar{w}_4(\bar{x}, \bar{y}) \end{aligned} \tag{15}$$

The functions $u_i(\bar{t})$ are the step functions which are zero at $\bar{t} < 0$ and one at $\bar{t} \geq 0$. The $u_i(\bar{t})$ are related to $a_i(\bar{t})$ through a limiting process of superposition of many infinitesimal step functions. The superposition will be implemented in the form of a convolution integral. The integrated pressure distribution $p_i(\bar{x}, \bar{y}, \bar{t})$ which arises from a unit step increase in nondimensional upwash $u_i(\bar{t})\bar{w}_i(\bar{x}, \bar{y})$ is the indicial response function $f_{i,j}(\bar{t})$:

$$f_{i,j}(\bar{t}) = \int\int_A p_i(\bar{x}, \bar{y}, \bar{t})\bar{x}^{m_j}\bar{y}^{n_j}\, dA \tag{16}$$

In other words, the simulation is performed four times in order to obtain the response to unit step increases in $\bar{w}_i$ and $p_i(\bar{x}, \bar{y}, \bar{t})$ is the pressure which arises with $u_i(\bar{t})\bar{w}_i(\bar{x}, \bar{y})$.

The convolution integral (Duhamel's theorem) uses the indicial response $f_{i,j}(\bar{t})$ to produce the lift which arises with any time function $a_j(\bar{t})$. The load $F_{1,j}(\bar{t})$ which arises with arbitrary plunging motion $\dot{a}_1(\bar{t})$ is

$$F_{1,j}(\bar{t}) = \int_{-\infty}^{\bar{t}} f_{1,j}(\bar{t} - \bar{\tau})\ddot{a}_1(\bar{\tau})\, d\bar{\tau} \tag{17}$$

The load $F_{2,j}(\bar{t})$ which arises with arbitrary pitching motion $\dot{a}_2(\bar{t})x$ is

$$F_{2,j}(\bar{t}) = \int_{-\infty}^{t} [f_{2,j}(\bar{t} - \bar{\tau})\ddot{a}_2(\bar{\tau}) + f_{1,j}(\bar{t} - \bar{\tau})\dot{a}_2(\bar{\tau})]\, d\bar{\tau} \tag{18}$$

Likewise, for chordwise and spanwise bending

$$F_{3,j}(\bar{t}) = \int_{-\infty}^{\bar{t}} [f_{3,j}(\bar{t} - \bar{\tau})\ddot{a}_3(\bar{\tau}) + 2f_{2,j}(\bar{t} - \bar{\tau})\dot{a}_3(\bar{\tau})]\, d\bar{\tau} \tag{19}$$

$$F_{4,j}(\bar{t}) = \int_{-\infty}^{\bar{t}} f_{4,j}(\bar{t} - \bar{\tau})\ddot{a}_4(\bar{\tau})\, d\bar{\tau} \tag{20}$$

Consider the harmonic constraint

$$a_j(\bar{t}) = A_j e^{ik\bar{t}} \tag{21}$$

where reduced frequency $k = \omega b/U$. (Note: ik is an imaginary number not to be confused with index i.) Then

$$\int_{-\infty}^{\bar{t}} f_{i,j}(\bar{t} - \bar{\tau})\dot{a}_j(\bar{\tau})\, d\bar{\tau} = A_j e^{ik\bar{t}}\left[f_{oi,j} + ik\int_0^{\infty} \hat{f}_{i,j}(\bar{\tau})e^{-ik\bar{\tau}}\, d\bar{\tau}\right] \tag{22}$$

$$\begin{aligned} &\int_{-\infty}^{\bar{t}} f_{i,j}(\bar{t} - \bar{\tau})\ddot{a}_j(\bar{\tau})\, d\bar{\tau} \\ &\quad = A_j e^{ik\bar{t}}\left[ikf_{oi,j} - k^2\int_0^{\infty} \hat{f}_{i,j}(\bar{\tau})e^{-ik\bar{\tau}}\, d\bar{\tau}\right] \end{aligned} \tag{23}$$

where the steady-state portion f_0 of the indicial response $f_{i,j}(\bar{t})$ has been considered separately:

$$f_{i,j}(\bar{t}) = f_{oi,j} + \hat{f}_{i,j}(\bar{t}) \tag{24}$$

The convolution integrals [Eqs. (22) and (23)] can be evaluated numerically.

Results

The first test case is an AGARD standard aspect ratio 1.45 tapered wing with 39-deg leading-edge sweep and a taper ratio (tip chord/root chord) of 0.709 at Mach 0.80. In all cases, the TDP method has taken advantage of symmetry about the wing centerline. All the test cases presented here were computed on a DEC Vaxstation 3. This is a 2.7 MIPS workstation with 71 Mbytes of usable formatted disk memory.

The discretized planform is depicted in Fig. 1 with a 15 × 15 grid. The harmonic loads were extensively documented in Ref. 12 where this wing is identified as planform no. 3. Here, five different "collocation" methods were compared at various values of reduced frequency. Reference 3 (computer pro-

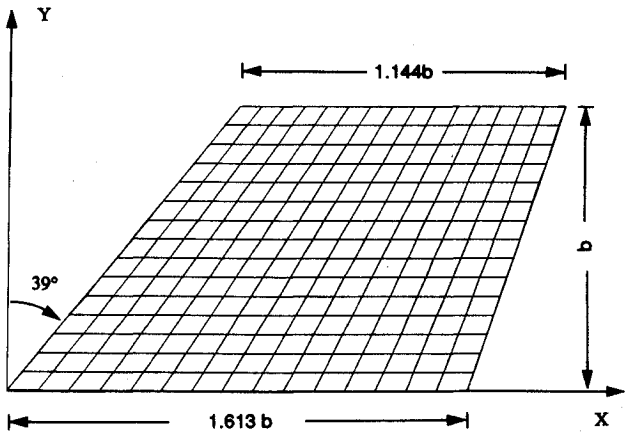

Fig. 1 Discretized AGARD wing planform (half-span).

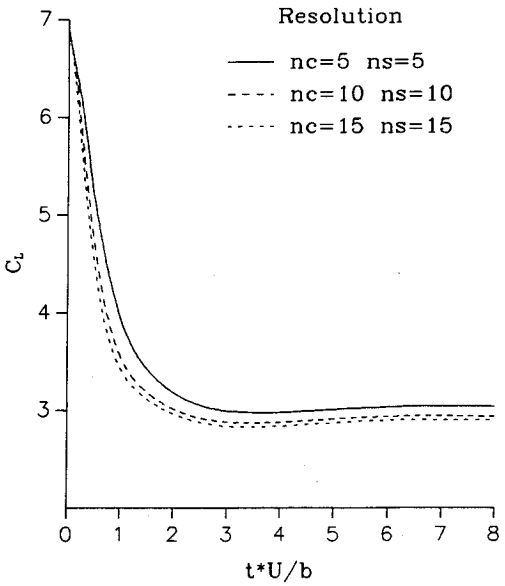

Fig. 2 AGARD wing indicial lift/plunge function (M = 0.8).

gram H7WC as implemented in the FASTOP or FASTEX program) is used here to represent the doublet-lattice method. As stated, the TDP method is not constrained to harmonic motion. The results from the TDP computer program are transformed to the frequency domain in order to correlate with results obtained with H7WC.[3]

The indicial response $f_{1,1}(\bar{t})$ is given in Fig. 2. This is the lift due to a step increase in plunge rate $[\bar{w}(\bar{x}, \bar{y}, \bar{t}) = u_1(\bar{t})]$. Nondimensional time ($\bar{t} = Ut/b$) is plotted on the horizontal axis. For this case, $\bar{t} = 1$ represents a distance traveled equal to the reference length b, the semispan. Nondimensional lift $C_L = 2 \times L/(\rho U^2 b^2)$ is plotted on the vertical axis. At $\bar{t} = 0$, the exact piston theory value is obtained from Eq. (5a) with $(\partial h/\partial x) = I_2 = 0$. Three results are plotted for different grid densities. In the legend of Fig. 2, *nc* denotes the number of chordwise panels, and *ns* denotes the number of spanwise panels. As was identified in Ref. 7, the indicial function is comprised of two parts, the noncirculatory and circulatory. The noncirculatory term is associated with $(\partial h/\partial t)$, and the circulatory term is associated with $(\partial h/\partial x)$ in Eq. (10). In the initial portion (when t is small) of the indicial function of Fig. 2, the noncirculatory term (piston theory) dominates. After the noncirculatory effect dies out, the circulatory term dominates.

Discretization errors are manifested in at least two ways. First, in the simulation of Fig. 2, a coarser grid is less able to model a sharp wave front than a finer grid. The discretization allows numerical disturbances to propagate instantaneously across each panel during each time step. For instance, given five chordwise panels, only five time steps are required for the effects of the trailing edge to "numerically propagate" upstream and influence the leading edge. Physically, more than 25 time steps are required for the time step used. Secondly, the steady-state solution differs slighty amoung the three curves. The final solution in each case exactly matches the steady-state value obtained by enforcing constant doublet strength with respect to time and directly solving Eq. (8) with a single matrix inversion. The convergence of the steady-state solution with grid refinement will be addressed later.

The time to create the $[A]$ matrix of Eq. (8) is about 30 min for the 15 × 15 case, about 5 min for the 10 × 10 case, and about 30 s for the 5 × 5 case. The time to simulate the indicial response on the Vaxstation 3 is substantially longer. The 5 × 5 case takes about 1.4 s/time step in computing a 4 × 4 matrix of indicial response functions $f_{i,j}(\bar{t})$. Likewise, the 10 × 10 case takes about 1.9 s/time step, and the 15 × 15 case takes about 40 s/time step. The 15 × 15 case is dominated by paging (a process of reading and writing on the disk for lack of random access memory). It is expected that this process could be hastened with more efficient programming and some simple approximations to the wake. One should take note that this algorithm is well-suited for parallel pro-

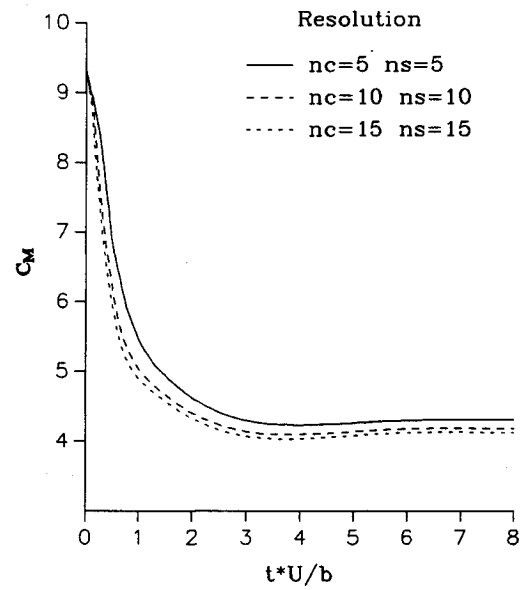

Fig. 3 AGARD wing indicial pitch moment/pitch function (M = 0.8).

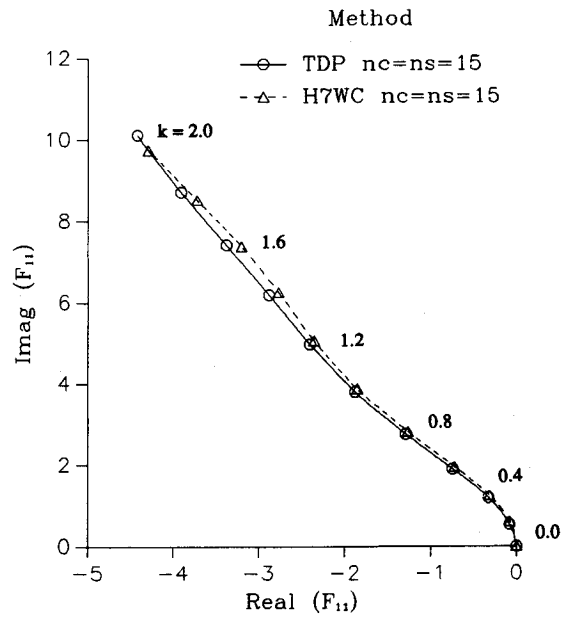

Fig. 4 AGARD wing lift/plunge harmonic correlation (M = 0.8).

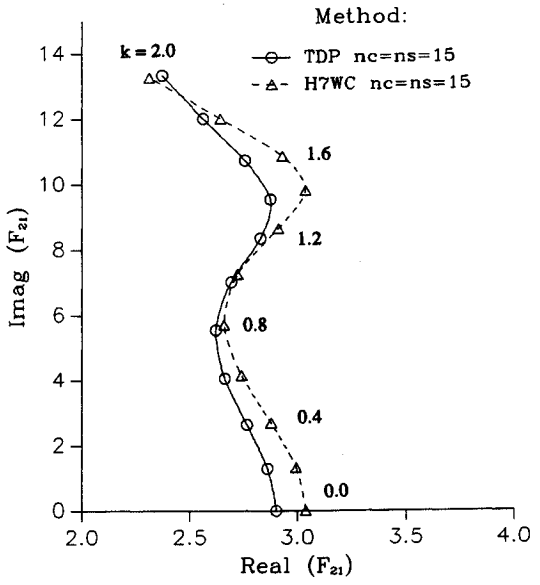

Fig. 5 AGARD wing lift/pitch harmonic correlation (M = 0.8).

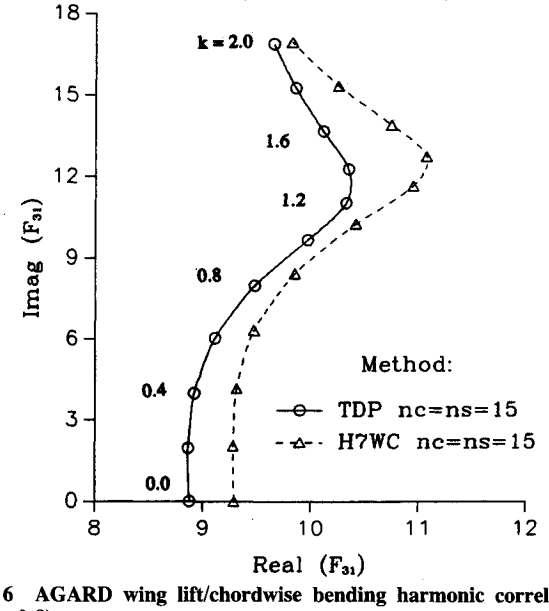

Fig. 6 AGARD wing lift/chordwise bending harmonic correlation (M = 0.8).

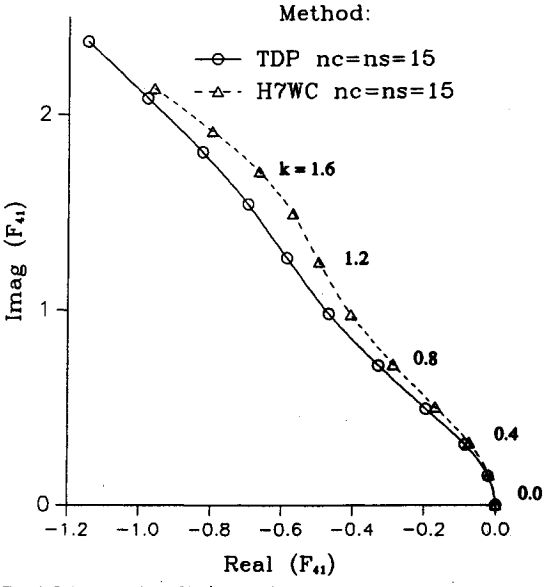

Fig. 7 AGARD wing lift/spanwise bending harmonic correlation (M = 0.8).

cessing. Tremendous speeds could be obtained with a parallel processor and the added complications are easily addressed.

Figure 3 records the indicial response to $\bar{w}_2(x, y)$. One draws the same conclusions here as with Fig. 2.

Figure 4 correlates the harmonic lift from H7WC and the transformed indicial response from TDP. In both cases, the lift due to constant amplitude plunge displacement is plotted at various reduced frequencies (k) based on the semispan. Correlation is excellent across the reduced frequency range investigated.

Figures 5–7 represent the same conditions and use the same format as in Fig. 4 to correlate H7WC and TDP. In each of these figures the lift is plotted at 11 reduced frequencies in increments of 0.2 over the range $0.0 \leq k \leq 2.0$. Figure 5 represents lift due to constant pitch amplitude $F_{2,1}$. Figure 6 represents lift due to constant chordwise bending (x^2) amplitude $F_{3,1}$. Figure 7 represents lift due to constant spanwise bending (y^2) amplitude $F_{4,1}$. Note the magnified real scale in Fig. 5. Therefore, the apparent difference here is not as great as it would appear with an expanded scale.

The sensitivity of these results to panel density is examined next. In all cases $ns = nc$ and $M = 0.8$. The wake is truncated along a line which is perpendicular to the axis of symmetry and crosses the wing centerline at 4.94 root chords aft of the wing leading vertex. Figure 8 is a graph of $F_{2,1}(t)$ at $k = 0$

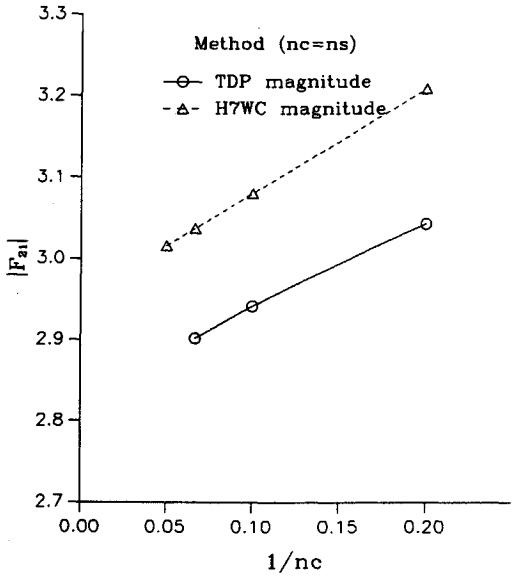

Fig. 8 AGARD wing lift/pitch convergence (k = 0.0).

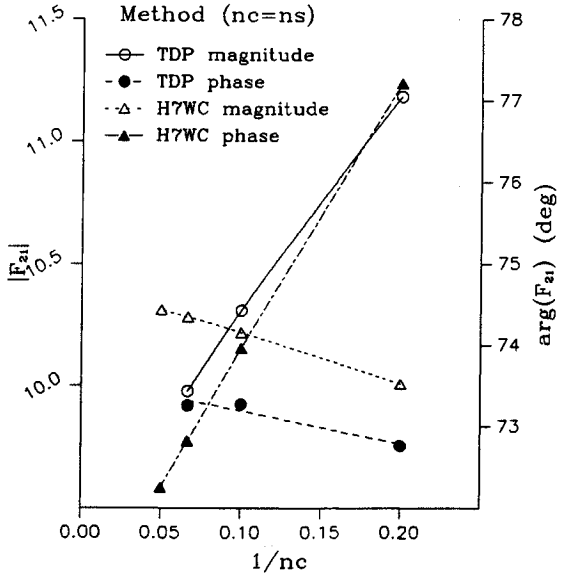

Fig. 9 AGARD wing lift/pitch convergence (k = 1.4).

for various refinements of the discretization. H7WC seems to converge to a value of about $F_{2,1} = 2.95$, and the TDP method seems to converge to about $F_{2,1} = 2.81$, about a 5% difference. Because the two schemes are attempting to solve the same boundary value problem, they should yield the same limiting solution. The reason for this difference is not understood at the present. Extending the wake to 25 root chords decreases $F_{2,1}$ by 0.02% for the 5 × 5 case.

Figure 9 depicts the results of a convergence study of $F_{2,1}$ for unsteady case $k = 1.4$. As in Fig. 8, the horizontal axis is $1/nc$. The limit for H7WC appears to be magnitude 10.4 and phase 70.5 deg, whereas that for TDP appears to be magnitude 9.3 and phase 73.5 deg. The difference in the converged solutions is larger than for the steady-state case. Again, the reason for the difference is not understood at the present time.

The second example is an aspect ratio two (AR2) rectangular wing at Mach 0.5. Figure 10 depicts this wing with a 15 × 15 grid. The wake is truncated five chords aft of the trailing edge. Similar simulations were performed with this rectangular wing as with the swept wing of Fig. (1). Some additional details are given in Ref. 13. Some important results are shown in Figs. 11 and 12.

Figure 11 is a graph of $F_{2,1}(t)$ at $k = 0$ for various refinements of the discretization. H7WC seems to converge to a value of about $F_{2,1} = 2.593$, and the TDP method seems

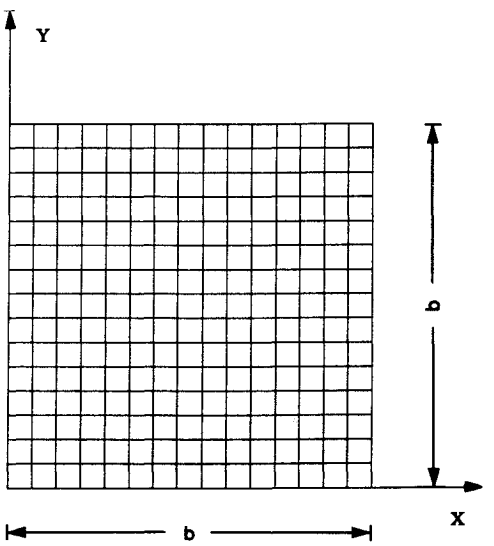

Fig. 10 Discretized AR2 wing planform (half-span).

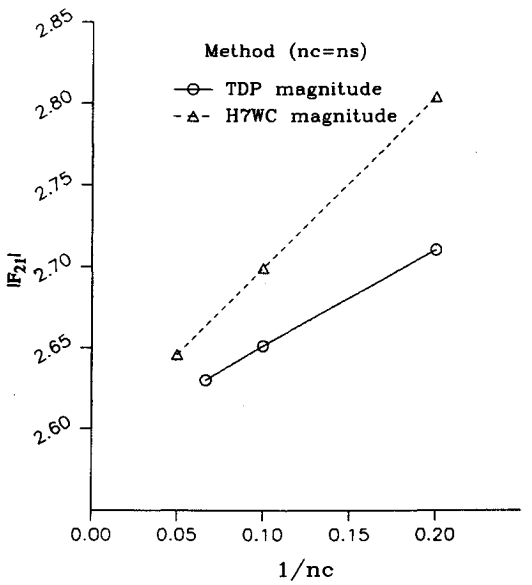

Fig. 11 AR2 wing lift/pitch convergence ($k = 0.0$).

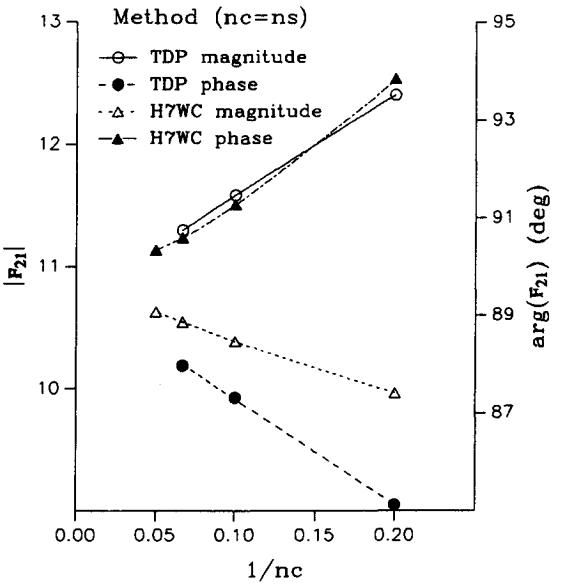

Fig. 12 AR2 wing lift/pitch convergence ($k = 1.4$).

to converge to about $F_{2,1} = 2.588$, about a 0.2% difference. This is a great improvement over the swept wing case. Furthermore, it is observed that for a given value of $nc \neq 0$, the TDP method is closer to the converged solution than is H7WC.

Figure 12 is a convergence study of $F_{2,1}$ at $k = 1.4$. Convergence for H7WC appears to be magnitude 10.87 and phase 90.00 deg. Convergence for TDP appears to be magnitude 10.73 and phase 89.44 deg. Again, the agreement is better than that produced with the swept wing case. Here, H7WC appears to converge sooner than the TDP method. It is interesting that the solutions converge from opposite directions. Flutter-speed predictions with both H7WC and TDP may offer high and low approximations, which are useful in assessing a particular design.

Conclusions

The integral formula of Ref. 1 has been implemented in a computer program. For the rectangular wing, the TDP and doublet-lattice[3] methods appear to give nearly the same limiting answers. The TDP method may offer better accuracy at low frequency for a finite discretization. For the swept wing, correlation is not as good as for the rectangular wing case. Although no conclusive explanation has been obtained yet, the following possibilities are under consideration. For the doublet-lattice method, the limiting solution depends on the location of the control points within the lattice. The doublet-lattice method is based on the three-quarter chord concept for a rectangular wing. This concept cannot be rigorously applied to swept or tapered wings. The choice of control point location is not unique. Another possible source of discrepancy is the effect of truncating the wake in the TDP method. However, a parameter study (not presented in this article) showed that the effect of wake truncation in the TDP method is not sufficient to account for the lack of agreement in the swept case. One avenue not taken is to employ a higher order steady-state panel method for the swept wing case. A convergence study for lift due to steady-state pitch could be compared to that presented in Fig. 8.

The TDP method is recommended for unsteady subsonic compressible aeroelastic analyses where a time domain dynamic simulation is part of the analysis. This approach is more direct than the process of obtaining time domain aerodynamics from harmonic aerodynamics such as Ref. 3. One disadvantage is the increased amount of data storage required.

Acknowledgments

M. Blair expresses his appreciation for both the support and leadership which K. G. Guderley has provided during

the past years. In addition, this author is grateful for the careful guidance provided by his thesis coadvisor, M. H. Williams, in areas related to the TDP method.

References

[1]Guderley, K. G., and Blair, M., "The Integral Equation for the Time Dependent Linearized Potential Flow over a Wing," AFWAL-TR-86-3077, Wright-Patterson AFB, OH, Dec. 1986.

[2]Williams, M. H., Guderley, K. G., and Lee, M. R, "An Alternative Derivation for an Integral Equation for Linearized Subsonic Flow over a Wing," WRDC-TR-89-3097, Wright-Patterson AFB, OH, Aug. 1989.

[3]Giesing, J. P., Palman, T. P., and Rodden, W. P., "Subsonic Unsteady Aerodynamics for General Configurations," AFFDL-TR-71-5, Wright-Patterson AFB, OH, Nov. 1971.

[4]Noll, T. E., Blair, M., and Cerra, J., "An Aeroservoelastic Analysis Method for Analog or Digital Systems," *Journal of Aircraft*, Vol. 23, No. 11, 1986, pp. 852–858.

[5]Blair, M., "Development and Application of the Time Domain Panel Method," Ph.D. Dissertation, Purdue Univ., West Lafayette, IN, Dec. 1989.

[6]Blair, M., Williams, M. H., and Weisshaar, T. A., "Time Domain Simulations of a Flexible Wing in Subsonic, Compressible Flow," 31st Structures, Structural Dynamics, and Materials Conf., AIAA 90-1153, Long Beach, CA, April 1990.

[7]Lomax, H., Heaslet, M. A., Fuller, F. B., and Sluder, L., "Two- and Three-Dimensional Unsteady Lift Problems in High Speed Flight," NACA Rept. 1077, 1952.

[8]Morino, L., "A General Theory of Unsteady Compressible Potential Aerodynamics," NASA CR-2464, Dec. 1974.

[9]Long, L. N., and Watts, G. A., "Arbitrary Motion Aerodynamics Using an Aeroacoustic Approach," *AIAA Journal*, Vol. 25, No. 11, 1987, pp. 1442–1448.

[10]Long, L. N., "The Compressible Aerodynamics of Rotating Blades Based on an Acoustic Formulation," NASA-TP-2197, Dec. 1983.

[11]Garrick, I. E., "Nonsteady Wing Characteristics," *Aerodynamic Components of Aircraft at High Speeds*, Sec. F, *High Speed Aerodynamics and Jet Propulsion*, Vol. 7, Princeton Univ. Press, Princeton, NJ, 1957.

[12]Woodcock, D. L., "A Comparison of Methods Used in Lifting Surface Theory," Supplement to Pt. VI of the *Manual on Aeroelasticity*, Royal Aircraft Establishment, AGARD-R-583-71, Farnborough, Hampshire, UK, June 1971.

[13]Blair, M., and Williams, M. H., "A Time Domain Panel Method for Wings," 30th Structures, Structural Dynamics, and Materials Conf., AIAA 89-1323, Mobile, AL, April 1989.